

α -Fe₂O₃ and Fe₃O₄ hollow nanospheres as high-capacity anode materials for rechargeable Li-ion batteries

Manickam Sasidharan · Nanda Gunawardhana ·
Masaki Yoshio · Kenichi Nakashima

Received: 5 December 2011 / Revised: 17 February 2012 / Accepted: 4 April 2012 / Published online: 5 May 2012
© Springer-Verlag 2012

Abstract α -Fe₂O₃ and Fe₃O₄ hollow nanospheres of size 30±2 nm were synthesized by using polymeric micelles as a soft template for the first time. The hollow nanospheres were thoroughly characterized by transmission electron microscope, superconducting quantum interference device, X-ray diffraction, Fourier transform infrared spectroscopy, thermogravimetry and differential thermal analysis, cyclic voltammogram, and nitrogen sorption analyses. The α -Fe₂O₃ and Fe₃O₄ hollow nanospheres were used as anode materials in lithium-ion rechargeable batteries to investigate their electrochemical properties. The hollow particle-based electrodes exhibit high capacity, stable cycling performance, and good rate capability at different current densities. The α -Fe₂O₃ and Fe₃O₄ hollow nanospheres with nanosized shell domain favors fast lithium insertion/extraction processes during the repeated charge/discharges.

Keywords Hematite · Magnetite · Hollow nanosphere · Anode material · Li-ion battery

Electronic supplementary material The online version of this article (doi:10.1007/s11581-012-0716-x) contains supplementary material, which is available to authorized users.

M. Sasidharan · K. Nakashima (✉)
Department of Chemistry, Faculty of Science and Engineering,
Saga University,
1 Honjo-Machi,
Saga 840-8502, Japan
e-mail: nakashik@cc.saga-u.ac.jp

N. Gunawardhana · M. Yoshio
Advanced Research Center, Saga University,
1341 Yogamachi,
Saga 840-0047, Japan

M. Yoshio
e-mail: yoshio@cc.saga-u.ac.jp

Introduction

Developing Li-ion batteries (LIBs) with high specific capacities and high current densities as power sources for diverse applications is of great interest [1–4]. The development of next-generation LIBs is a key to the success of electric and hybrid electric vehicles, advanced electronic devices, and implantable medical devices [1, 5, 6]. Since the pioneering work of Poizot and co-workers in the year 2000 on the reversible full reduction of 3D metal oxides, the research on α -Fe₂O₃ electrode has gained much interest [7]. Iron oxide, one of the main components of the earth's crust, is considered to be a potential candidate with a high charge/discharge current densities and high reversible capacity coupled with its low cost and environmental benignity. Stimulated by both the promising applications of iron oxides coupled with novel properties of nanosize, considerable efforts have been made in the synthesis of α -Fe₂O₃ nanoparticles, nanorods, nanowires, and nanotubes [8–14]. Investigation by Larcher et al. and Morales et al. on Fe₂O₃ nanoparticles and by Chen et al. and Zhang et al. on carbon-coated Fe₃O₄ nanospindles has clearly proved that the morphology of nanosized particles plays a significant role in the reactivity of the electrode materials toward lithium [15–17]. In addition, it has been proved that the electrochemical reaction of Li with Fe₂O₃ is thermodynamically feasible, and up to 6 mol of Li can be intercalated to give a maximum theoretical capacity of 1,007 mAh g⁻¹ [17]. Similarly, Fe₃O₄ can accommodate up to 8 mol of Li making them promising anode materials for high-performance lithium-ion batteries.

Recently, polymeric micelles with *core-shell-corona* structure have increasingly used for the fabrication of hollow nanospheres [18]. The micelle of poly(styrene-*b*-2-vinylpyridine-*b*-ethylene oxide) (PS-PVP-PEO), consisting of a PS *core*, a PVP *shell*, and a PEO *corona* was used

as a soft template in the fabrication of hollow silica nanospheres in our laboratory. Herein, we report on the fabrication of hollow α - Fe_2O_3 and Fe_3O_4 nanospheres with micelles of poly(styrene-*b*-acrylic acid-*b*-ethylene oxide) (PS-PAA-PEO) using $\text{FeCl}_3 \cdot 6\text{H}_2\text{O}$ as iron precursor. The importance of this strategy is that the PS *core* functions as template for hollow void, PAA *shell* domain containing anionic $-\text{COO}^-$ ions serves as effective reaction center for metal ions, and PEO *corona* stabilizes the particles from aggregation. In the present report, the precursor metal cations (Fe^{3+}) are first precipitated on the anionic PAA block with COO^- groups in the form of hydroxides, and this phase is subsequently transformed to porous α - Fe_2O_3 hollow nanospheres by calcinations in air atmosphere. The α - Fe_2O_3 hollow spheres further converted to magnetite hollow nanospheres by controlled reduction with a mixture of H_2 and N_2 at 350 °C. To the best of our knowledge, this is the first report for the synthesis of magnetic hollow nanospheres of size about 30 nm using soft template strategy. Both α - Fe_2O_3 and Fe_3O_4 nanospheres were further investigated as anode materials for their electrochemical lithium intercalation/deintercalation behaviors in rechargeable LIBs.

Experimental

Material preparation and characterization The α - Fe_2O_3 hollow nanospheres were fabricated as depicted in Scheme 1. The micelle solution was adjusted to pH 8 by using dilute NaOH solution. The required amount of micelle solution (10 mL) was stirred for a few minutes followed by addition of $\text{FeCl}_3 \cdot 6\text{H}_2\text{O}$ under vigorous stirring (the ratio of Fe^{3+} /PAA was 10). Then dilute NH_4OH was added slowly until the pH is reached to about 10 and the obtained brown precipitate was aged for 2 days at room temperature under static conditions. The composite particles were repeatedly washed with distilled water and ethanol and dried at 60 °C. In order to remove the polymeric template as well as to crystallize the hollow particles, the composite particles were heated to 400 °C for 3 h in a muffle furnace under air. The α - Fe_2O_3 hollow nanospheres obtained by the above method were further reduced to Fe_3O_4 hollow nanospheres using a mixture of H_2 and N_2 at 350 °C for 2 h. Prior to transformation of Fe_2O_3 to Fe_3O_4 hollow

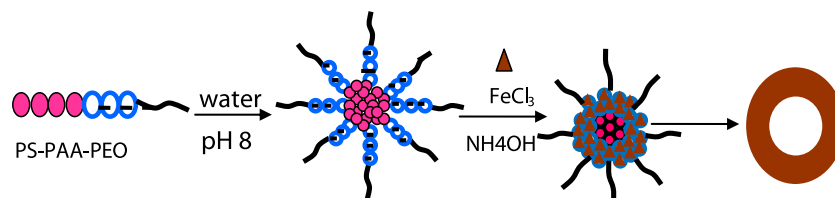
nanospheres, the suitable reduction temperature (350 °C for 2 h) was identified since high temperature (above 450 °C) leads to total reduction of Fe^{3+} to a certain extent. Wide-angle X-ray diffraction (XRD) was recorded on a Shimadzu XRD-7000 (WXRD) diffractometer. N_2 adsorption/desorption analyses were carried out by using an Autosorp I apparatus. Transmission electron microscope (TEM) images were recorded on JEOL JEM-1210 (80 kV) and JEM-2100 (200 kV) electron microscopes. Fourier transform infrared (FTIR) spectra were recorded on a Jasco FT/IR 7300 spectrometer by using a KBr pellet technique. Thermogravimetry and differential thermal analysis (TG-DTA) were obtained with a MAC Science TG-DTA 2100 instrument under air. The magnetic measurement was made on Quantum Design SQUID MPMS-XL instrument, and temperature-dependant magnetization data were obtained at 5,000 Oe

Electrode preparation For lithium insertion studies in lithium-ion batteries, the $\text{Fe}_2\text{O}_3/\text{Fe}_3\text{O}_4$ nanosphere (5 mg) was mixed mechanically with teflonized acetylene black (2 mg), and then the mixture was pressed on a stainless steel mesh as the current collector under a pressure of 500 kg/cm^2 and dried at 160 °C for 4 h under vacuum. The electrochemical characterizations were carried out using CR-2032 coin-type cells with pure lithium (Cyprus Foote Mineral Co.) as an anode. The electrolyte used was 1 M LiPF_6 -EC/DMC (1:2 by volume, Ube Chemicals Co. Ltd.). The coin cell assembling was performed in a glove box filled with argon (dew point, lower than -80 °C). Cyclic voltammograms (CVs) were recorded by Hokuto denko HSV-100 (Japan) in a beaker-type cell which contains Fe_2O_3 or Fe_3O_4 working electrode, and lithium foil acts as both reference and counter electrodes. The beaker-type cell was assembled in the argon filled glove box and sealed well using Teflon seal tape to prevent air oxidation.

Results and discussion

The fabrication of Fe_2O_3 and Fe_3O_4 hollow nanospheres using PS-PAA-PEO micelles is depicted in Scheme 1. On gradual addition of FeCl_3 solution to the above micelles, the anionic PAA *shell* block effectively binds with Fe^{3+} ions

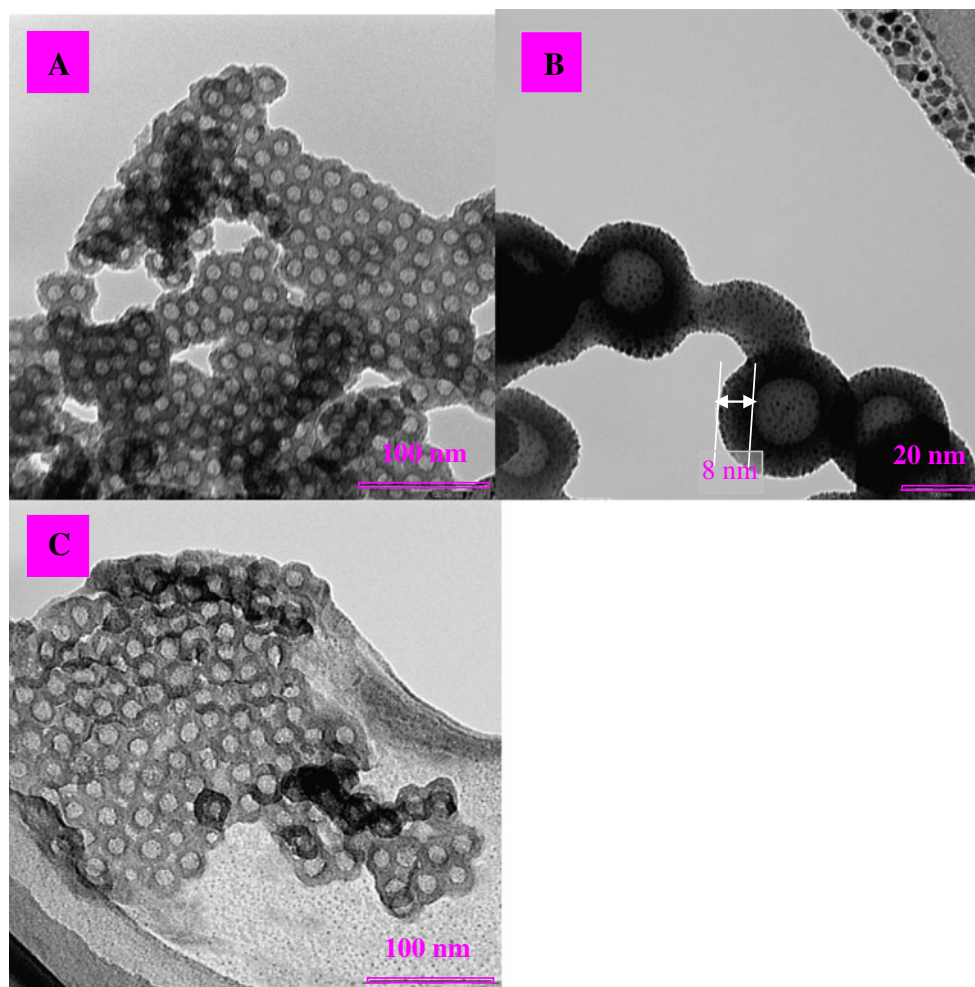
Scheme 1 Fabrication of Fe_2O_3 and Fe_3O_4 hollow nanospheres using micelles



through electrostatic interaction as shown in the Scheme 1. The charge neutralization between $-\text{COO}^-$ and Fe^{3+} ions also confirmed from change in the ξ -potential from -36 to 0 mV with gradual addition of FeCl_3 to the micelle solution (Fig. S1, supporting information). Thermal analyses (TG/DTA) of iron oxide/polymer composite particles (prior to calcinations) indicated that most of the templates were decomposed below 400 °C (Fig. S2, supporting information). The FTIR spectrum of composite particles (Fig. S3-A, supporting information) containing $-\text{COO}-\text{Fe}^{3+}$ complex exhibits bands at $1,737$ and $1,456$ cm^{-1} corresponding to asymmetric and symmetric stretching vibration of $-\text{COO}^-$, respectively. The FTIR spectra of $\alpha\text{-Fe}_2\text{O}_3$ and Fe_3O_4 materials exhibited bands at 580 , 850 – $1,040$, and $1,600$ cm^{-1} characteristic of Fe–O bond vibrations (Fig. S3B–C, supporting information) [19]. The absence of C–H, $-\text{C}=\text{C}-$, and $-\text{COOH}$ bonds stretching vibrations of phenyl groups of the polymer backbone in the calcined sample suggests the complete removal of templates from the hollow nanospheres. Furthermore, thermal analysis of calcined samples revealed negligible amount of organics in the Fe_2O_3 hollow particles. Figure 1a, c shows the TEM images of $\alpha\text{-Fe}_2\text{O}_3$ and Fe_3O_4

hollow nanospheres, respectively; the average particle size and void space diameter of hollow nanospheres were found to be 30 ± 2 and 15 ± 1 nm, respectively; the reduction of $\alpha\text{-Fe}_2\text{O}_3$ to Fe_3O_4 has not affected the spherical morphology of particles. All the hollow particles are polycrystalline, and the shell domain is comprised of nanoparticles of diameter about 2 – 4 nm as evidenced from the high-resolution TEM images (Fig. 1b). The wall thickness estimated from TEM images was found to be 8 ± 0.5 nm. Figure 2 shows the powder XRD patterns of nanosized hollow iron oxides; the XRD profile prior to hydrogen treatment matches well with the standard $\alpha\text{-Fe}_2\text{O}_3$ (JCPDS 33-0664) [20, 21]. After reduction, the crystalline structures could be indexed to Fe_3O_4 (JCPDS 75-1609). All detected sharp diffraction peaks could be indexed as Fe_3O_4 , and the absence of peak at $2\theta=44^\circ$ clearly confirms the absence of metallic iron (Fe^0) [21]. It is important to note that controlled reduction at low temperature (at 350 °C for 2 h) avoids Fe metal formation unlike the high-temperature treatment using H_2 . Furthermore, the $\alpha\text{-Fe}_2\text{O}_3$ hollow nanospheres were completely converted to Fe_3O_4 because the peaks unique for $\alpha\text{-Fe}_2\text{O}_3$ (including the peaks at 24.1 , 33.08 , and 40.86) disappeared completely. The formation of

Fig. 1 TEM images of hollow nanospheres: **a** $\alpha\text{-Fe}_2\text{O}_3$ (low magnification), **b** $\alpha\text{-Fe}_2\text{O}_3$ (high magnification), and **c** Fe_3O_4



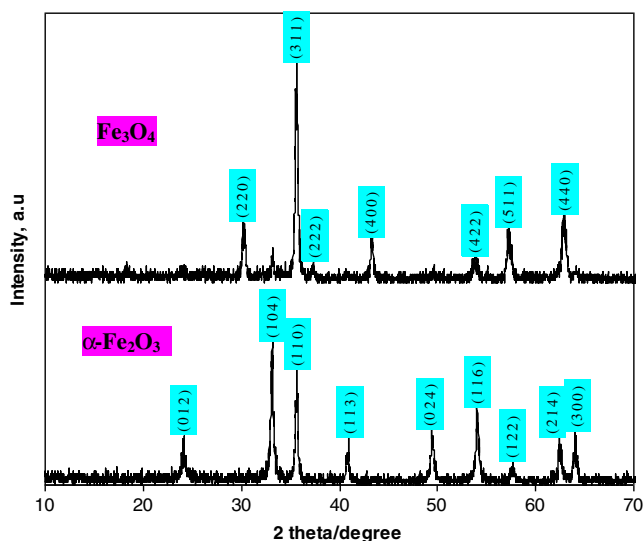


Fig. 2 Wide-angle XRD patterns of α - Fe_2O_3 and Fe_3O_4 hollow nanospheres

Fe_3O_4 is further confirmed by the color change from brown to totally black materials.

The Brunauer–Emmett–Teller surface areas evaluated by nitrogen adsorption/desorption analyses of α - Fe_2O_3 and Fe_3O_4 hollow nanospheres were found to be 106 and 93 $\text{m}^2 \text{g}^{-1}$, respectively. Magnetic characterization was performed using a superconducting quantum interference device (SQUID). The temperature-dependant magnetization at 5,000 Oe for Fe_3O_4 hollow particles is shown in the supporting information (Fig. S4). The hollow Fe_3O_4 nanospheres are superparamagnetic at room temperature. The hollow particles exhibited a magnetic moment of 22.3 emu/g which is comparable to values obtained by Sun et al. for Fe_3O_4 hollow nanospheres of size about 20–25 nm [21]. Furthermore, the decrease in magnetic susceptibility with decreasing temperature indicates the hollow nanospheres become antiferromagnetic at low temperature, and the antiferromagnetism increases with decreasing temperature up to 2 K. The Néel temperature (T_N), the critical temperature for onset of antiferromagnetism, is observed at about 200 K characteristics of magnetite particles [22].

Figure 3a, b shows discharge–charge curves in the voltage window of 0.005–3.0 V (vs. Li) at a rate of 0.25 C up to 50 cycles, and for clarity, only selected cycles are shown in the voltage versus capacity profiles. During the first discharge, both α - Fe_2O_3 and Fe_3O_4 exhibit voltage plateaus at about 1.1 and 0.8 V (vs. Li) resulting from the lithium reaction with iron oxide nanospheres [14, 17]. The voltage plateau at 1.1 continues until a capacity of about $220 \pm 20 \text{ mAh g}^{-1}$ is reached for both hametite and magnetite which is ascribed to Li insertion into the shell domain of hollow nanospheres, whereas the voltage plateau at 0.8 V continuing up to 950 mAh g^{-1} reflects the reduction of Fe^{3+}

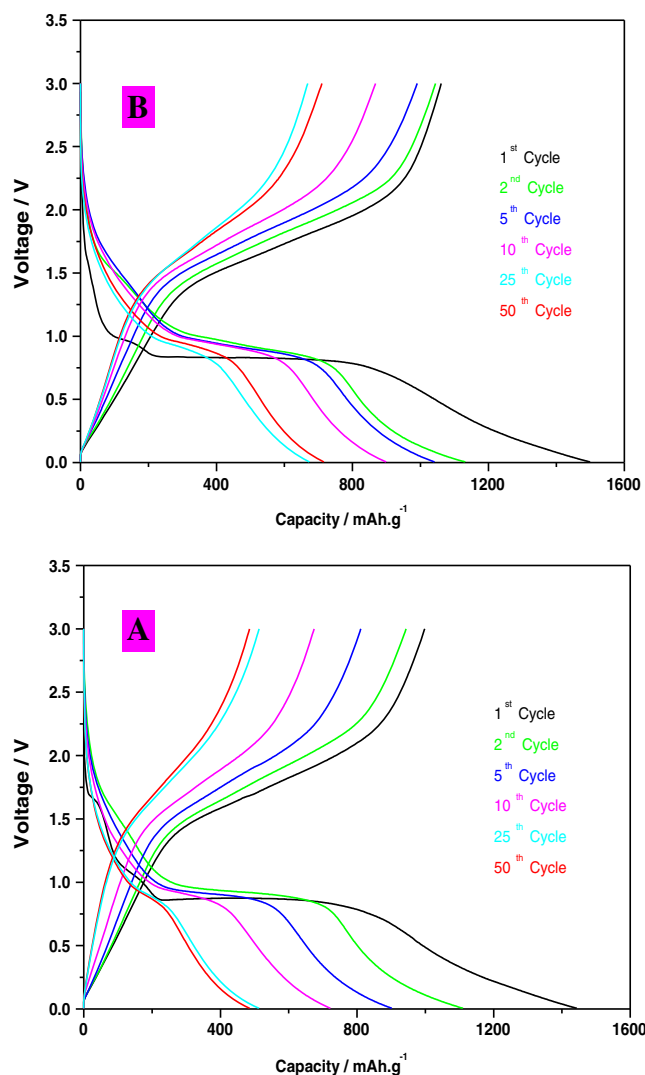


Fig. 3 Charge/discharge profiles of α - Fe_2O_3 (a) and Fe_3O_4 (b) hollow nanospheres at 0.25 C rate in the potential region of 0.005–3.0 V vs. Li/Li^+

to Fe^0 metal clusters [16]. The charge curve showed a sloping plateau at 1.95 V due to reverse oxidation reaction of $\text{Fe}^0 \rightarrow \text{Fe}^{3+}$. The total first-discharge capacity is $1,430 \pm 10 \text{ mAh g}^{-1}$ which corresponds to 8.6 mol of Li/mol of Fe_2O_3 , whereas Fe_3O_4 exhibited slightly higher discharge capacity $1,495 \text{ mAh g}^{-1}$ (9.0 mol Li/mol of Fe_3O_4) at similar experimental conditions. The first-discharge profiles of both hametite and magnetites qualitatively resemble that observed by Larcher et al. and Morales et al. on Fe_2O_3 nanoparticulate and Chen et al. on Fe_2O_3 nanotubes [14–17]. It is noteworthy to mention that in the complete reduction of $\text{Fe}^{3+} \rightarrow \text{Fe}^0$, one would expect a maximum uptake of 6 Li/ Fe_2O_3 or 8 Li/ Fe_3O_4 ($1,005 \text{ mAh g}^{-1}$), and the excess capacity must originate from electrolyte decomposition in the low-potential region and subsequent formation of solid electrolyte interphase on the hollow nanospheres [23, 24].

The discharge capacities of the α -Fe₂O₃ electrode (Fig. 3a) in the 1st, 2nd, 5th, 10th, 25th, and 50th cycles are 1,435, 1,109, 895, 681, 518, and 490 mAh g⁻¹, respectively. The corresponding charge capacity values are 998, 943, 811, 650, 503, and 485 mAh g⁻¹ for the 1st, 2nd, 5th, 10th, 25th, and 50th cycles, respectively. The coulombic efficiency of first cycle was found to be 69.5 %. The corresponding capacity versus cycle number plot is shown in Fig. 4a. As can be seen, both discharge and charge capacities decrease up to 15 cycles and thereafter the capacity stabilizes. After 50 cycles with 100 % depth of discharging and charging at a rate of 0.25 C, the electrode capacity decreased to 485 mAh g⁻¹. The capacity retention of Fe₂O₃ from 15th to 50th cycle is 84.2 %. Similar charge/discharge cycling performance was also observed on α -Fe₂O₃ nanotube electrodes and nanoflakes embedded on copper foil [17, 25]. Furthermore, it is relevant to mention that the capacity of commercial α -Fe₂O₃ faded within few cycles to 250 mAh g⁻¹ and gradually decreased to about 130 mAh g⁻¹ in less than 50 cycles [26]. However, the

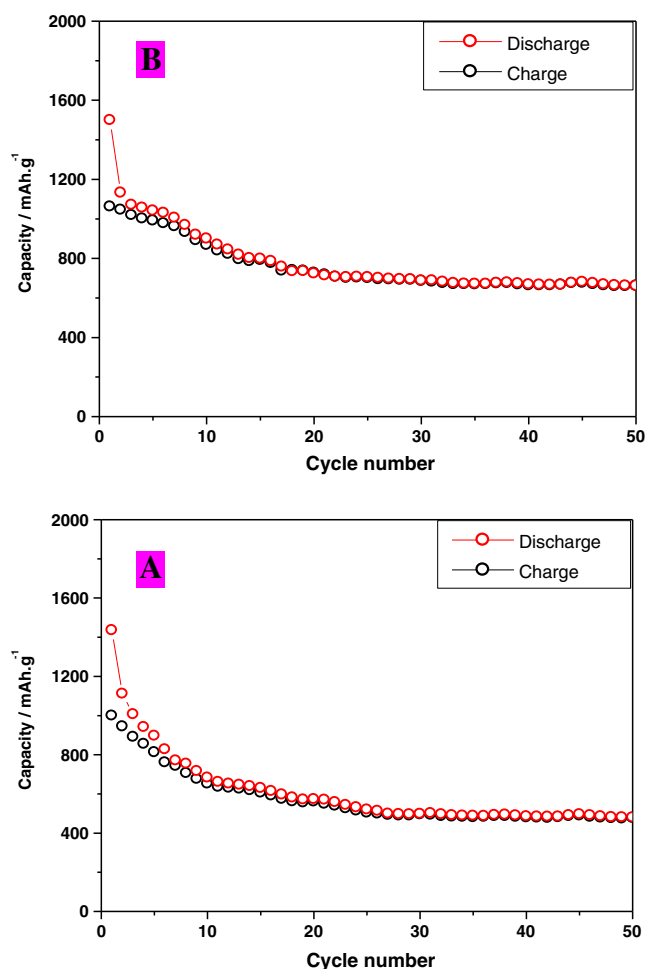


Fig. 4 Charge/discharge cycling performance of α -Fe₂O₃ (a) and Fe₃O₄ (b) hollow nanospheres at 0.25 C rate in the voltage region of 0.005–3.0 V vs. Li/Li⁺

performance of α -Fe₂O₃ hollow nanospheres in the present study is more than three times higher than that of commercial Fe₂O₃ and porous α -Fe₂O₃ nanotubes in the absence of any additives [27].

The magnetite (Fe₃O₄) hollow nanospheres, however, exhibit enhanced charge/discharge capacities (Fig. 3b) compared to α -Fe₂O₃. The discharge capacity values (Fe₃O₄) at 0.25 C rate in the voltage window of 0.005–0.3 V (vs. Li) for 1st, 2nd, 5th, 10th, 25th, and 50th cycles are 1,498, 1,139, 1,041, 890, 694, and 690 mAh g⁻¹, respectively. The corresponding charge capacity values of Fe₃O₄ are 1,060, 1,044, 990, 867, 695, and 688 mAh g⁻¹ for the 1st, 2nd, 5th, 10th, 25th, and 50th cycles, respectively. The coulombic efficiency of first cycle was found to be 71 %, marginally higher than the α -Fe₂O₃ hollow nanospheres. The cycling performance of Fe₃O₄ (Fig. 4b) also shows similar behavior as that of α -Fe₂O₃ and the discharge capacities decrease up to 15 cycles possibly due to the formation of stable electrolyte film, and complete coverage of all hollow nanoparticles may require several charge/discharge cycles and similar observation was also noticed by other groups [14–17]. The observed discharge capacity after 50 cycles (690 mAh g⁻¹) for Fe₃O₄ hollow nanospheres is considerably higher than the carbon/Fe₃O₄ nanospindles (600 mAh g⁻¹) composite electrodes, where the Fe₃O₄ nanoparticles were mixed with carbon matrix [25]. However, it is worth to note that carbon/Fe₃O₄ electrode delivers 600 mAh g⁻¹ after 80 cycles. On comparison with commercial Fe₃O₄ nanoparticles, which fades quickly and as a result provides low capacity (152 mAh g⁻¹, after 50 cycles) [26], the Fe₃O₄ hollow nanospheres exhibit 4.5 times higher discharge capacity than the commercial Fe₃O₄. The capacity fading may be partly due to volume change during repeated charge/discharges similar to Sn- and Si-based anodes [28]. The difference in electrochemical performance of α -Fe₂O₃ and Fe₃O₄ with nearly similar size 30±2 nm is attributed to the intrinsic electronic conductivities of latter which contribute to higher discharge/charge capacities and superior performance than the α -Fe₂O₃ [29]. This fact is further confirmed from the enhanced performance of Fe₃O₄/single-walled carbon nanotubes (SWNT) due to high electronic conductivity of these composite electrodes containing SWNT [30]. Therefore, one can expect still improved performance of Fe₃O₄ hollow nanospheres when mixed with appropriate carbon additives. At this juncture, we are investigating the performance of synthesized Fe₂O₃ and Fe₃O₄ with different carbon additives. We believe this may enhance the initial coulombic efficiency and cyclability.

Figure 5a, b shows the rate performances of α -Fe₂O₃ and Fe₃O₄ hollow nanospheres, respectively. At a low rate of 0.15 C (Fe₃O₄, charge–discharge of all active materials in period of 400 min) or 0.1 C (Fe₂O₃), both α -Fe₂O₃ and Fe₃O₄ show about 1,100 to 1,150 mAh g⁻¹. However, at a

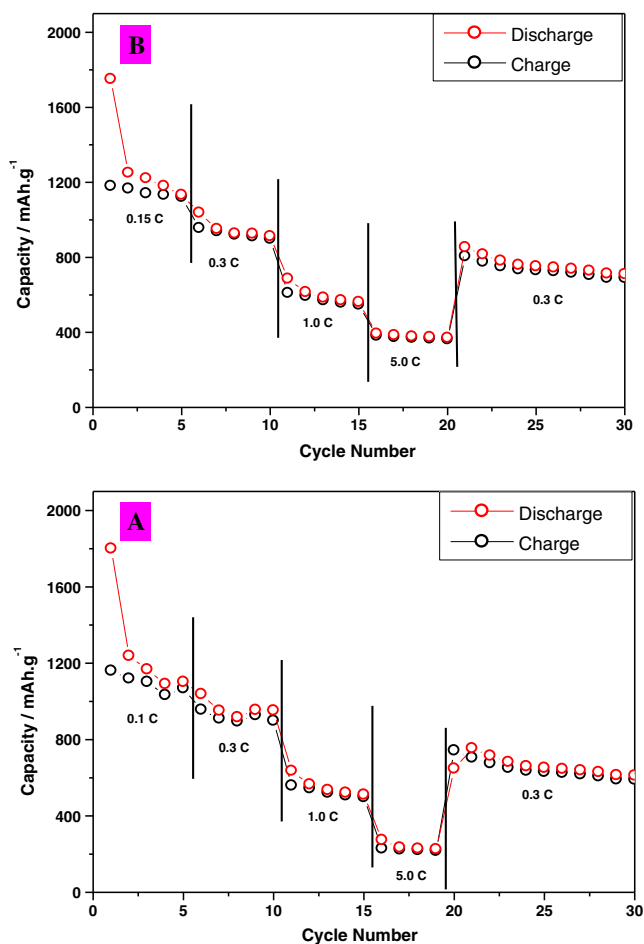


Fig. 5 Rate performance of α -Fe₂O₃ (a) and Fe₃O₄ (b) of hollow nanospheres at different rates in the voltage region of 0.005–3.0 V vs. Li/Li⁺

high rate of 5 C (discharge/charge of all active materials within 12 min), the specific capacity of α -Fe₂O₃ decreases to 265 mAh g⁻¹, whereas that of Fe₃O₄ reduced to 410 mAh g⁻¹ at the same rate of 5 C. Thus, consistency with other nanostructured materials with different morphologies, the iron oxide hollow particles also show higher capacity at slower rate (0.1 C) than that at faster rate (5 C). However, the α -Fe₂O₃ and Fe₃O₄ electrodes almost regain their original high capacities when the rate was again lowered to 0.3 C after being exposed to high current loads (5 C), which indicates the high stability of hollow nanosphere-based electrodes. The improved electrochemical performance of both Fe₂O₃ and Fe₃O₄ is attributed partially to the unique hollow spherical morphology. More importantly, the void space not only effectively buffers against charge storage and local volume change but also provides better electrical contact and shorter diffusion path length providing better rate capability. In addition, enhanced capacity retention, rate performance, and cycling performance of Fe₃O₄ over Fe₂O₃ hollow nanospheres are solely attributed to inherent electronic conductivities of magnetite

particles. Figure 6 shows the CVs of α -Fe₂O₃ and Fe₃O₄ in the potential window 0.005–3 V (vs. Li⁺/Li) at a scan rate of 3 mV/min. During the first cycle, a smooth sloping curve (cathodic) up to about 0.8 V with shoulders at 1.68 and 1.1 V is indicative of insertion of Li and reduction of Fe³⁺ in α -Fe₂O₃ in the shell domain of hollow nanospheres. The appearance of a strong oxidation peak at 1.6 V suggests the oxidation of Fe⁰ to Fe³⁺ ions. The second cathodic sweep differs from the first one; the shoulders at 1.68 and 1.1 V appeared in the first scan vanished in the second cycle. The cyclic voltammogram of Fe₃O₄ is slightly different from Fe₂O₃ (Fig. 6b). In the cathodic polarization process of the first cycle, a reduction peak appeared at 0.5 V corresponding to Li insertion and reduction of Fe³⁺ to metallic iron. However, the oxidation scanning exhibited two peaks at 1.55 and 2.14 V indicating the oxidation of Fe⁰ to Fe²⁺ and then to Fe³⁺. The second cathodic sweep exhibited an additional shoulder at 1.5 V, and essentially the peak positions are unaltered with subsequent cycles.

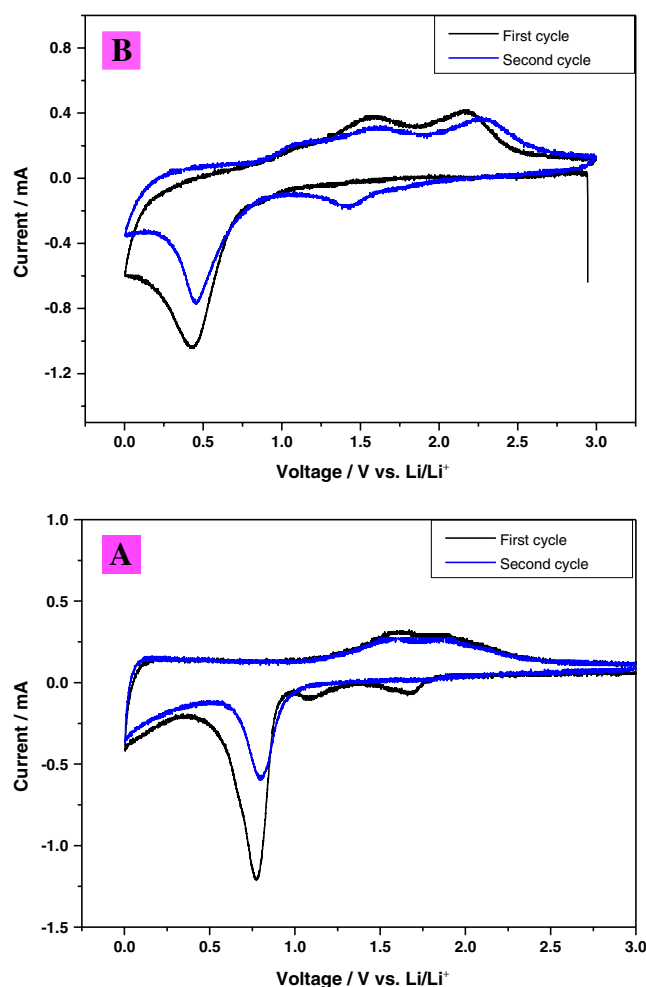


Fig. 6 Cyclic voltammogram of hollow nanospheres: a α -Fe₂O₃ and b Fe₃O₄ in 1.0 M LiPF₆ (EC/DMC=1/2 (v/v)) at a 3-mV/min sweep rate

Conclusions

In summary, we have demonstrated a simple soft template method for fabrication of α - Fe_2O_3 and Fe_3O_4 hollow nanospheres of size 30 ± 2 nm with void space of about 14–15 nm. Fe_3O_4 hollow particles exhibited a magnetic moment of 22.5 emu/g as estimated by SQUID. The charge/discharge cycling performance and rate performance α - Fe_2O_3 hollow nanospheres were comparable to that of α - Fe_2O_3 nanotube and nanoflakes coated on conducting copper foil. Fe_3O_4 hollow nanospheres exhibited higher discharge capacity after 50 cycles (690 mAh g^{-1}) which is considerably higher than the carbon/ Fe_3O_4 nanospindles (600 mAh g^{-1}) composite electrodes and commercial Fe_3O_4 . The Fe_3O_4 nanospheres show 4.5 times higher discharge capacity than the commercial materials, and the improved rate performance is attributed partially to the unique hollow spherical morphology coupled with hollow void space. The void space not only acts as buffer medium against charge storage and local volume change but also provides better electrical contact and shorter diffusion path length and therefore provides better rate capability.

Acknowledgments One of the authors (KN) thanks the Japan Society for the Promotion of Science for a Grant-in-Aid for Scientific Research (20310054).

References

1. Armand M, Tarascon JM (2008) *Nature* 451:652
2. Li N, Martin CR, Scrosati B (2001) *J Power Sources* 97–98:240
3. Wang H, Abe T, Maruyama S, Iriyama Y, Ogumi Z, Yoshikawa K (2005) *Adv Mater* 17:2857
4. Park M, Kang Y, Wang G, Dou S, Liu H (2008) *Adv Funct Mater* 18:455
5. Chen J, Cheng F (2009) *Acc Chem Res* 42:713
6. Jiang C, Hosono E, Zhou H (2006) *NanoToday* 1:28
7. Poizot P, Laruelle S, Grugeon S, Dupont L, Tarascon JM (2000) *Nature* 407:496
8. Xu XN, Wolfus Y, Shaulov A, Yeshurun Y, Felner I, Nowik I, Kolytyn Y, Gedanken A (2002) *Appl Phys Lett* 91:4611
9. Ji J, Ohkoshi S, Hashimoto K (2004) *Adv Mater* 16:48
10. Woo K, Lee HJ, Ahn JP, Park YS (2003) *Adv Mater* 20:1761
11. Wang X, Chen X, Gao L, Zheng Z, Ji M, Tang C, Sen T, Zhang Z (2004) *J Mater Chem* 14:905
12. Fu YY, Wang RM, Xu J, Chen J, Yan Y, Narlikar AV, Zhang H (2003) *Chem Phys Lett* 379:373
13. Shen XP, Liu HJ, Pan L, Chen KM, Hong JM, Xu Z (2004) *Chem Lett* 33:1128
14. Larcher D, Masquelier C, Bonnin D, Chabre Y, Masson V, Leriche JB, Tarascon JM (2003) *J Electrochem Soc* 150:A133
15. Larcher D, Bonnin D, Rivals I, Personnaz L, Tarascon JM (2003) *J Electrochem Soc* 150:A1643
16. Morales L, Sanchez L, Martin F, Berry F, Ren X (2005) *J Electrochem Soc* 152:A1748
17. Chen J, Xu L, Li W, Gou X (2005) *Adv Mater* 17:582
18. Khanal A, Inoue Y, Yada M, Nakashima K (2007) *J Am Chem Soc* 129:1534
19. Tan H, Xue JM, Shuter B, Li X, Wang J (2010) *Adv Funct Mater* 20:722
20. Bang JH, Suslick KS (2007) *J Am Chem Soc* 129:2242
21. Peng S, Sun S (2007) *Angew Chem Int Ed* 46:4155
22. Yi DK, Selvan ST, Lee SS, Papaefthymiou GC, Kundaliya D, Ying JY (2005) *J Am Chem Soc* 127:4990
23. Xing WB, Dahn JR (1997) *J Electrochem Soc* 144:1195
24. Mukai SR, Hasegawa T, Takagi M, Tamon H (2004) *Carbon* 42:837
25. Zhang WM, Wu XL, Hu JS, Guo YG, Wan LJ (2008) *Adv Funct Mater* 18:3941
26. Tartaj P, Amarilla JM (2011) *J Power Sources* 196:2164
27. Guo YG, Hu YS, Sigle W, Maier J (2007) *Adv Mater* 19:2087
28. Aifantis KE, Huang T, Hackney SA, Sarakonsri T, Yu A (2012) *J Power Sources* 197:246
29. Taberna PL, Mitra S, Poizot P, Simon P, Tarascon JM (2006) *Nat Mater* 5:567
30. Ban C, Wu Z, Gillaspie DT, Chen L, Yan Y, Blackburn JL, Dillion AC (2010) *Adv Mater* 22:E145